

Alignment effects in the medium-spin level structure of ^{78}Se

K. Mandal,^{1,2} A. Chakraborty^{1,*} A. K. Mondal,^{1,3} U. S. Ghosh¹ Aniruddha Dey,¹ Saumyajit Biswas^{1,4},
B. Mukherjee¹ S. Rai^{1,5} S. Chatterjee,⁶ S. K. Das,⁶ S. Samanta,⁶ R. Raut⁶,⁶ S. S. Ghugre,⁶ S. Bhattacharyya,^{7,8}
S. Nandi^{7,8} S. Bhattacharya,^{7,8} G. Mukherjee^{7,8} S. Ali,⁹ A. Goswami,^{9,†} S. Mukhopadhyay¹⁰ Krishichayan^{11,12}
R. Banik^{8,13} R. Chakrabarti,¹⁴ V. Kumar,¹⁵ and A. Kumar¹⁵

¹Department of Physics, Siksha Bhavana, Visva-Bharati University, Santiniketan, West Bengal 731 235, India

²Department of Physics, Chandidas Mahavidyalaya, Khujutipara, West Bengal 731 215, India

³Department of Physics, Bolpur College, Bolpur, West Bengal 731 204, India

⁴Department of Physics, Murshidabad College of Engineering and Technology, Banjelia, West Bengal 742 102, India

⁵Forensic Science Laboratory, 37/1/2 Belgachia Road, Kolkata 700 037, India

⁶UGC-DAE Consortium for Scientific Research, Sector III, LB-8, Bidhan Nagar, Kolkata 700 106, India

⁷Variable Energy Cyclotron Centre, Sector I/AF, Bidhan Nagar, Kolkata 700 064, India

⁸Homi Bhabha National Institute, Training School Complex, Anushakti Nagar, Mumbai 400 094, India

⁹Saha Institute of Nuclear Physics, I/AF, Bidhan Nagar, Kolkata 700 064, India

¹⁰Nuclear Physics Division, Bhabha Atomic Research Centre, Trombay, Mumbai 400 085, India

¹¹Department of Physics, Duke University, Durham, North Carolina 27708, USA

¹²Triangle Universities Nuclear Laboratory, Durham, North Carolina 27708, USA

¹³Institute of Engineering and Management, Saltlake Sector V, Kolkata 700091, India

¹⁴Department of Physics, University of Mumbai, Vidyanaigari, Mumbai 400 098, India

¹⁵Department of Physics, Banaras Hindu University, Varanasi 221 005, India



(Received 13 January 2021; revised 6 January 2022; accepted 2 March 2022; published 25 March 2022)

The excited states of ^{78}Se were populated using the $^{76}\text{Ge}(\alpha, 2n)$ fusion evaporation reaction. The deexcited gamma rays were detected using the Indian National Gamma Array (INGA) spectrometer comprising clover and low-energy photon spectrometer (LEPS) detectors. The ground state band of ^{78}Se has been extended up to $E_x = 8.5$ MeV and $J = 16\hbar$; this excitation regime is very close to the $\pi(1g_{9/2}^2)$ crossing frequency. Several newly observed in-band and intraband transitions belonging to the other bands of ^{78}Se have also been placed in the level scheme based on their coincidence relationships. From the newly identified $E1$ transitions, an enhancement in the $B(E1)/B(E2)$ values with spin has been observed which indicates the onset of octupole correlations in the band structure built on the 3^- , 2508-keV state. Persistence of triaxial shape up to the highest observed spin of the ground state band has been observed and the feature of successive $1g_{9/2}^2$ quasiparticle alignments due to protons and neutrons has been unveiled. The consequences arising due to the occurrence of the neutron $1g_{9/2}$ quasiparticle alignments in the other observed correlated band structures are also presented. The results are interpreted in terms of total Routhian surface (TRS) calculations and the level structure systematic of the neighboring nuclei.

DOI: [10.1103/PhysRevC.105.034328](https://doi.org/10.1103/PhysRevC.105.034328)

I. INTRODUCTION

The shape transition phenomenon in the even-even nuclei belonging to the $A \approx 80$ mass region has been investigated by several groups over the past few decades. The level structures of most of the even-even Se and Kr isotopes lying in this mass region exhibit a distinct change of shape with increasing spin owing to the simultaneous as well as successive alignments of pairs of $1g_{9/2}$ proton and neutron quasiparticles [1–5]. The complexity in the level scheme at medium spin (with $J \approx 6\hbar$) arising due to the competing collective and quasiparticle excitation modes also provides interesting

physics issues which have been addressed through different theoretical model calculations. Prior to the present work, the level structure of ^{78}Se in the low- and medium-spin regime was determined using the $^{76}\text{Ge}(\alpha, 2n)$ fusion evaporation reaction by two different groups. The spectroscopic work of Matsuzaki *et al.* [6] established the level scheme up to $E_x = 4.6$ MeV with $J = 10\hbar$, and the back-bending phenomenon was studied. In the subsequent study by Schwengner *et al.* [7], the ground state level scheme of ^{78}Se was extended up to $E_x = 5.8$ MeV with $J = 12\hbar$. The later work provided evidence for the loss in collectivity of the ground state positive parity band above the 6^+ state. The reduction in collectivity of the ground state band was found to be due to the interaction of the band with $1g_{9/2}$ two-proton and two-neutron excitations. We point out here that the two-quasiparticle $\nu(1g_{9/2}^2)$ aligned states, corresponding to the first band crossing, in the positive

*anagha.chakraborty@visva-bharati.ac.in

†Deceased.

parity ground band of ^{78}Se were observed in both the previous studies. However, the results of the previous two investigations exhibit significant differences in terms of grouping of levels into different sideband structures, and the discrepancies among the spin-parity assignments for many of the levels can be seen. In addition, the spin-parity assignments could not be made for some of the levels in the previous studies.

The present gamma-ray spectroscopy work for ^{78}Se has aimed toward resolving the anomalies that persist among the results of the two previous works. For proper characterization of the sidebands, it is essential to search for the important intraband linking transitions and assign their firm multipolarities. For example, for proper characterization of the octupole correlated states built on the γ -vibrational states, it is very necessary to establish the connecting intraband transitions of $E1$ multipolarity. Furthermore, the much-delayed second band crossing phenomenon was found to occur along the positive parity ground state band of the neighboring ^{76}Se isotope [2], and a shape transition from prolate to oblate was considered to be the cause for the observed delayed $1g_{9/2}$ proton-pair alignment. On the other hand, the observed delay for the second band crossing in ^{74}Se [8] is much smaller than that of ^{76}Se . Occupying the intermediate position in the isotopic chain, it would be of interest to extend the ground state positive parity band of ^{78}Se in the higher spin regime so that the consequent effect of the second band crossing due to two-quasiparticle $\pi(1g_{9/2}^2)$ alignments can be studied.

Hence, the present investigation has been carried out with the alpha-induced $^{76}\text{Ge}(\alpha, 2n)$ fusion evaporation reaction, and a comparatively larger array comprising high-resolution clover Ge detectors has been used. It is worth mentioning that the previous measurements were performed using a limited number of Ge(Li) detectors. In the present investigation, the higher sensitivity and better resolving power of the array has been utilized for unambiguous placements of several weak inter- and intraband linking transitions. Firm spin-parity assignments for many of the levels could be made possible through coincidence angular anisotropy and polarization asymmetry measurements. Thus, it has become feasible to bring out a comprehensive level scheme of ^{78}Se in the medium- and high-spin regime from the present investigation, and the quasiparticle alignment effects in the newly extended ground state band and the sidebands have been reported.

II. EXPERIMENTAL PROCEDURE AND DATA ANALYSIS

The excited states of ^{78}Se were populated using the $^{76}\text{Ge}(\alpha, 2n)$ fusion-evaporation reaction. The 30 MeV α beam was obtained from the K-130 Cyclotron at VECC, Kolkata. The target was prepared through centrifuge process by depositing enriched ^{76}Ge (94% enrichment) powder on Mylar backing. The thickness of each target thus prepared was about 2 mg/cm². Two such targets were stacked together and used for the experiment in order to enhance the yield of the residual nuclei. The γ rays emitting from the excited states of the residual nuclei were detected using Indian National Gamma Array (INGA). The array comprised seven Compton-suppressed

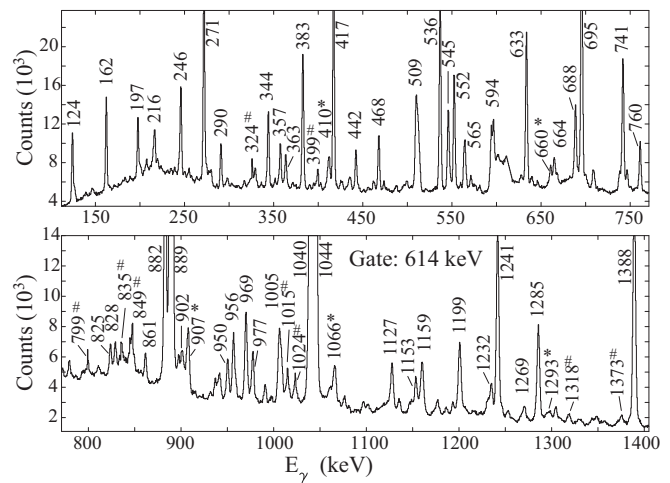


FIG. 1. Representative $\gamma\gamma$ coincidence spectrum with the gate sets on the 614($2^+ \rightarrow 0^+$)-keV ground-state-feeding transition of ^{78}Se . Peaks labeled with their energy values (in keV) have been assigned to ^{78}Se . The newly observed transitions are marked with *. The peaks marked with # are the contaminants from the neighboring residual nuclei, $^{77,76}\text{Se}$.

high-resolution clover detectors and one low-energy photon spectrometer (LEPS). Out of the seven clover detectors, four were placed at 90° , one was placed at 40° , and the remaining two were placed at 125° with respect to the beam direction. The LEPS used during the experiment has a single planar high-purity germanium (HPGe) crystal with four electrical segmentations and was placed at 40° . The data were recorded using a PIXIE-16 based digital data acquisition system [9]. A total of about 1.6×10^8 $\gamma\gamma$ coincidence events were recorded during the experiment. The offline data sorting process was carried out using the Linux based data sorting code IUCPIX [9]. The energy and efficiency calibrations of the detectors were carried out using the standard ^{152}Eu and ^{133}Ba radioactive sources. The data were sorted into the conventional $\gamma\gamma$ symmetric and asymmetric matrices for detailed offline analysis. The subsequent spectral analyses were carried out using RADWARE [10] and TV [11] software packages.

The representative $\gamma\gamma$ coincidence spectrum obtained by setting the gate on the strongest ground-state-feeding branch of the 614-keV ($2^+ \rightarrow 0^+$) transition of ^{78}Se is shown in Fig. 1. All the transitions reported in the previous works [6,7] are clearly seen in the spectrum. The spectrum also indicates the presence of a few contaminant transitions originating from the neighboring residual nuclei, $^{76,77}\text{Se}$. The data obtained from the present experiment suggest a good amount of yield for ^{77}Se , followed by ^{76}Se as well. The transitions that are newly assigned to ^{78}Se have been marked with *. The newly placed 1293-keV transition from the 7078-keV level in band 2 can also be seen in the spectrum with a limited peak intensity. Comparing the peak intensity of the 1293-keV transition, it appears that the coincidence peak intensity seen in the spectrum for the intense 1388-keV peak is mainly contributed from the 1388-keV transition of band 4 decaying from the low-lying 5^- , 2891-keV level, and the contribution from the newly placed 1388-keV transition originating from the

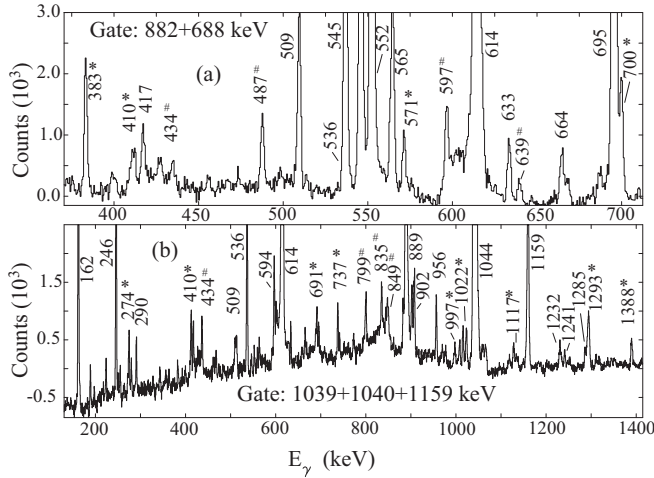


FIG. 2. Representative $\gamma\gamma$ coincidence spectra obtained from (a) the sum gates of 882- and 688-keV γ transitions of band 3 and (b) the sum gates of 1039-, 1040-, and 1159-keV transitions of band 2 of ^{78}Se . The peaks labeled with their energy values (in keV) have been assigned to ^{78}Se . The newly observed transitions are marked with *. The contaminant peaks from the neighboring $^{77,76}\text{Se}$ residual nuclei are marked with #.

high-lying 16^+ , 8466-keV level should be nominal. The majority of the transitions belonging to band 5 can also be seen from the coincidence spectrum of Fig. 1. The spectrum shown in Fig. 2(a) demonstrates the coincidence relationships among the transitions connected with bands 3 and 4. The position of the newly placed 1388-keV transition of band 2 is confirmed from the coincidence spectrum of Fig. 2(b).

The multiplicities of the transitions decaying from the excited states of ^{78}Se have been determined from the DCO (directional correlations from oriented states) ratio [12–14] and polarization asymmetry [14] measurements. In the present investigation, the value of R_{DCO} of a transition was extracted using the following relation:

$$R_{DCO} = \frac{I_{\gamma_1} \text{ at } 125^\circ \text{ gated with } \gamma_2 \text{ at } 90^\circ}{I_{\gamma_1} \text{ at } 90^\circ \text{ gate with } \gamma_2 \text{ at } 125^\circ}.$$

For extracting the R_{DCO} values, the $\gamma\gamma$ coincidence data have been sorted into an asymmetric matrix, one axis of which corresponds to the γ transitions recorded at the 90° detectors, and the other axis contains the data recorded by the detectors at 125° . The use of gating transitions with a stretched and pure multipole character (such as $E2$, $E1$, etc.) are preferable for extracting the R_{DCO} values of the transitions with unknown multiplicities. Hence, the R_{DCO} values of a majority of the transitions of ^{78}Se have been extracted using the 614($2^+ \rightarrow 0^+$)- and 889($4^+ \rightarrow 2^+$)-keV $E2$ gating transitions (see Table I). However, the R_{DCO} values for the weak interband connecting transitions could not be deduced from the 614- and 889-keV gating transitions. In those cases, the R_{DCO} values have been extracted using other adjacent gating transitions with known $E2$ multiplicities. The gating transitions used in the specific cases are listed in Table I. Figure 3 depicts the R_{DCO} values for the newly assigned multiplicities of the transitions of ^{78}Se . The figure clearly demonstrates a clear

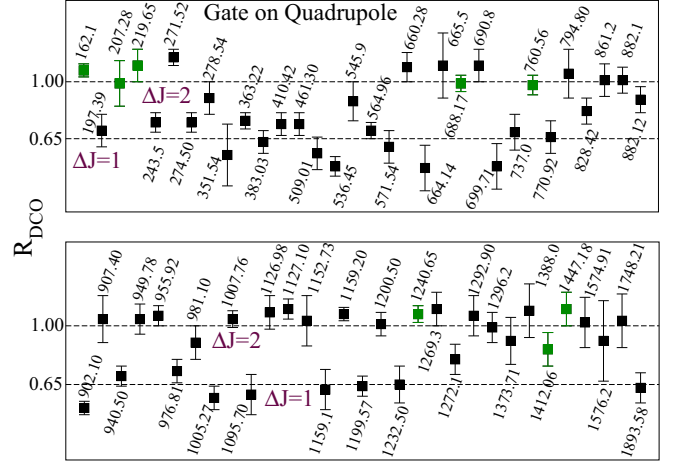


FIG. 3. The experimental R_{DCO} values for a few of the transitions belonging to ^{78}Se . The green data points correspond to the transitions with $\Delta J = 0$ character.

demarcation in R_{DCO} values for the transitions with $\Delta J = 1$ and $\Delta J = 2$ character. The $\Delta J = 1$ and $\Delta J = 2$ lines have been drawn to guide the eye. The position of the $\Delta J = 1$ line has been fixed with the weighted mean of the R_{DCO} values of several well known $E1$ transitions of $^{76,78}\text{Se}$ determined through the known stretched $E2$ gating transitions. The weighted average of the R_{DCO} value thus obtained is found to be 0.647 ± 0.013 , which corresponds to a value of $\sigma/J \approx 0.35$ (as obtained from the ANCOR code [15]) for the given geometry used while extracting the R_{DCO} values. This value of σ/J is consistent with the values determined for other alpha-induced fusion evaporation reactions [16]. For a typical $\Delta J = 0$ transition, the expected R_{DCO} value should in general be close to unity when a $\Delta J = 2$ transition is used as the gate. This behavior is similar to what one expects for a pure $\Delta J = 2$ transition. Such a behavior in R_{DCO} values for a few transitions can also be seen in the figure (see the green data points in Fig. 3).

The electromagnetic nature (electric or magnetic) of the transitions in ^{78}Se has been characterized from the polarization asymmetry (Δ_{asym}) values, defined as

$$\Delta_{\text{asym}} = \frac{a(E_\gamma)N_\perp - N_\parallel}{a(E_\gamma)N_\perp + N_\parallel},$$

where N_\perp and N_\parallel are the numbers of scattered photons in the directions perpendicular and parallel to the reaction plane, respectively. The term $a(E_\gamma)$ represents the geometrical asymmetry correction factor, and depends upon the geometry of the detectors as well as the array used for the measurements. The variation of $a(E_\gamma)$ [defined as $a(E_\gamma) = N_\parallel(\text{unpolarized})/N_\perp(\text{unpolarized})$]; the unpolarized ^{152}Eu radioactive source was used to determine the values of $N_\parallel(\text{unpolarized})$ and $N_\perp(\text{unpolarized})$] for a 90° clover detector as a function of energy of the transitions from ^{152}Eu has been fitted with the linear equation, $a = a_0 + a_1 E_\gamma$, and values of $a_0 = 1.002(10)$ and a_1 in the order of 10^{-6} were obtained.

TABLE I. Summary of the various spectroscopic quantities of ^{78}Se measured in the present investigation. The level energies (E_x^i) have been obtained by making a least-squares fit to the measured gamma-ray energies (E_γ) through the GTOL code [39]. The newly observed levels and transitions are highlighted with boldface. Unless otherwise stated, the assigned multiplicities to the gamma transitions are based on the deduced values of coincidence directional correlation ratio (R_{DCO}) and polarization asymmetry (Δ_{asym}) as obtained from the present investigation. The levels which have not been assigned to any particular sequence or bands of Fig. 5 are presented in italics. Only those transitions and levels are included for which additional information could be newly obtained from the present investigation. The quoted values of RI correspond to the relative intensities for the concerned transitions.

E_x^i (keV)	E_γ (keV)	RI	$J_i^\pi \rightarrow J_f^\pi$	R_{DCO}	Δ_{asym}	Multiplicity
1854.47(16)	351.54(20)	0.25(5)	$3^+ \rightarrow 4^+$	0.55(19) ^c		($M1 + E2$)
2190.99(17)	688.17(16)	3.2(2)	$4^+ \rightarrow 4^+$	0.99(5) ^b	-0.01(3)	$M1 + E2$
	882.12(20)	8.4(5)	$4^+ \rightarrow 2^+$	0.89(8) ^e	0.07(2)	$E2$
	1576.2(6)	0.8(1)	$4^+ \rightarrow 2^+$	0.91(24) ^e	0.07(4)	$E2$
2362.22(13) ^c	1748.21(60)	0.5(2)	$(0^+) \rightarrow 2^+$	1.03(16) ^a	0.12(10)	($E2$)
2508.34(17)	1005.27(22)	2.7(2)	$3^- \rightarrow 4^+$	0.57(7) ^a	0.06(3)	$E1$
	1199.57(20)	5.5(3)	$3^- \rightarrow 2^+$	0.64(6) ^a	0.08(4)	$E1$
	1893.58(60)	2.2(2)	$3^- \rightarrow 2^+$	0.63(9) ^a	0.06(4)	$E1$
2629.9(3)	1126.98(36)	4.7(3) ^b	$(6^+) \rightarrow 4^+$	1.08(10) ^f	0.04(3)	($E2$)
2682.73(24)	828.42(30)	0.40(8)	$4^+ \rightarrow 3^+$	0.82(8) ^a	-0.09(11)	$M1 + E2$
	1373.71(50)	0.67(6)	$4^+ \rightarrow 2^+$	0.91(14) ^d	0.08(10)	$E2$
2736.53(19)	545.9(2)	0.80(6)	$5^+ \rightarrow 4^+$	0.88(12) ^k	-0.03(5)	$M1 + E2$
	882.1(2)	8.4(5)	$5^+ \rightarrow 3^+$	1.01(8) ^f	0.07(1)	$E2$
	1232.50(56)	2.0(2)	$5^+ \rightarrow 4^+$	0.65(11) ^a	-0.11(4)	$M1 + E2$
2743.12(18)	234.1(3)	0.10(1)	$4^- \rightarrow 3^-$			[$M1 + E2$]
	1240.65(45)	3.2(3)	$4^- \rightarrow 4^+$	1.07(5) ^b	-0.07(3)	$E1$
2890.77(18)	147.75(30)	0.07(1)	$5^- \rightarrow 4^-$			[$M1 + E2$]
	699.71(27)	0.9(1)	$5^- \rightarrow 4^+$	0.48(14) ^c	0.10(7)	$E1$
2915.0(6)	1412.06(50)	0.41(11)	$4^+ \rightarrow 4^+$	0.86(10) ^b	0.07(7)	$M1 + E2$
2950.30(21)	207.28(31)	0.27(3)	$4^- \rightarrow 4^-$	0.99(14) ^c		($M1 + E2$)
	1095.70(44)	0.6(1)	$4^- \rightarrow 3^+$	0.59(12) ^a	0.06(5)	$E1$
	1447.18(60)	0.7(1)	$4^- \rightarrow 4^+$	1.1(1) ^b	-0.06(8)	$E1$
3014.79(20)	271.52(18)	6.2(3)	$6^- \rightarrow 4^-$	1.15(5) ^a	0.07(4)	$E2$
	278.54(44)	0.27(2)	$6^- \rightarrow 5^+$	0.9(1) ^c		($E1$)
3088.12(23)	197.39(20)	0.34(2)	$6^{(-)} \rightarrow 5^-$	0.7(1) ^a		($M1 + E2$)
3140.86(21)	949.78(29)	3.4(2)	$6^+ \rightarrow 4^+$	1.04(9) ^a	0.07(5)	$E2$
3307.73(19)	219.65(20)	0.24(2)	$6^- \rightarrow 6^{(-)}$	1.1(1) ^h		($M1 + E2$)
	571.54(25)	0.61(5)	$6^- \rightarrow 5^+$	0.6(1) ^h	0.10(6)	$E1$
	760.56(28)	2.3(1)	$6^- \rightarrow 6^+$	0.98(6) ^h	-0.11(4)	$E1$
3487.6(5)	940.50(44)	0.71(6)	$(7^-) \rightarrow 6^+$	0.70(6) ^b	0.09(6)	($E1$)
3523.89(20)	383.03(33)	0.70(5)	$7^- \rightarrow 6^+$	0.63(7) ^e	0.10(7)	$E1$
	509.01(24)	3.5(2)	$7^- \rightarrow 6^-$	0.56(10) ⁱ	-0.04(3)	$M1 + E2$
	976.81(30)	2.8(2)	$7^- \rightarrow 6^+$	0.73(7) ^j	0.08(4)	$E1$
3551.15(21)	243.5(3)	0.30(3)	$7^- \rightarrow 6^-$	0.75(6) ^o		($M1 + E2$)
	410.42(24)	0.26(3)	$7^- \rightarrow 6^+$	0.74(7) ^e		($E1$)
	536.45(27)	4.4(2)	$7^- \rightarrow 6^-$	0.48(6) ⁱ	-0.04(2)	$M1 + E2$
	660.28(25)	0.57(4)	$7^- \rightarrow 5^-$	1.09(9) ^o	0.08(7)	$E2$
3706.0(3)	564.96(34)	0.40(5)	$7^+ \rightarrow 6^+$	0.70(5) ^e	-0.03(6)	$M1 + E2$
	1159.1(4)	0.6(1)	$7^+ \rightarrow 6^+$	0.62(12) ^p		($M1 + E2$)
3831.74(25)	690.8(4)	0.26(2)	$8^+ \rightarrow 6^+$	1.1(1) ^e		($E2$)
4049.31(25)	525.41(50)	weak	$8^- \rightarrow 7^-$			[$M1 + E2$]
4122.2(3)	981.10(35)	0.35(4)	$8^+ \rightarrow 6^+$	0.90(10) ^e		($E2$)
	1574.91(52)	0.8(1)	$8^+ \rightarrow 6^+$	1.02(15) ^a	0.05(4)	$E2$
4214.96(24)	166.1(5)	weak	$8^- \rightarrow 8^-$			[$M1 + E2$]
	664.14(28)	0.68(4)	$8^- \rightarrow 7^-$	0.47(14) ⁱ	-0.05(4)	$M1 + E2$
	691.2(5)	weak	$8^- \rightarrow 7^-$			[$M1 + E2$]
	907.40(44)	0.30(3)	$8^- \rightarrow 6^-$	1.04(14) ^o		($E2$)
	1200.50(45)	1.12(6)	$8^- \rightarrow 6^-$	1.01(7) ⁱ	0.07(4)	$E2$
4293.0(4)	461.30(32)	0.46(5)	$(9^+) \rightarrow 8^+$	0.74(7) ^l	-0.04(3)	$M1 + E2$

TABLE I. (Continued.)

E_x^i (keV)	E_γ (keV)	RI	$J_i^\pi \rightarrow J_f^\pi$	R_{DCO}	Δ_{asym}	Multipolarity
4412.99(25)	198.94(31)	0.10(2)	$9^- \rightarrow 8^-$			[$M1 + E2$]
	363.22(28)	0.99(5)	$9^- \rightarrow 8^-$	0.76(5) ^b	-0.06(4)	$M1 + E2$
	581.1(4)	0.15(5)	$9^- \rightarrow 8^+$			[$E1$]
	861.2(5)	1.3(1)	$9^- \rightarrow 7^-$	1.01(10) ⁱ	0.07(6)	$E2$
	888.90(36)	3.6(2)	$9^- \rightarrow 7^-$	1.7(3) ⁿ	0.09(7)	$E2$
4626.1(3)	794.80(32)	0.50(5)	$10^+ \rightarrow 8^+$	1.05(15) ^l	0.09(8)	$E2$
4713.8(4)	1007.76(31)	1.04(7)	$9^+ \rightarrow 7^+$	1.04(5) ^f	0.05(4)	$E2$
4788.0(3)	162.1(2)	1.6(2)	$10^+ \rightarrow 10^+$	1.07(4) ^a		($M1 + E2$)
	665.5(4)	0.30(5)	$10^+ \rightarrow 8^+$	1.1(2) ^k		($E2$)
	955.92(30)	2.1(2)	$10^+ \rightarrow 8^+$	1.06(6) ^l	0.10(4)	$E2$
4820.2(3)	605.25(30)	0.14(1)	$9^- \rightarrow 8^-$			[$M1 + E2$]
	770.92(35)	0.34(3)	$9^- \rightarrow 8^-$	0.66(10) ^h		($M1 + E2$)
	1269.3(5)	0.60(4)	$9^- \rightarrow 7^-$	1.1(1) ⁱ	0.08(6)	$E2$
4858.9(3)	1296.2(5)	0.30(3)	$9^- \rightarrow 7^-$	0.99(9) ^g		($E2$)
	737.0(3)	0.67(5)	$9^+ \rightarrow 8^+$	0.69(11) ^l	-0.07(11)	$M1 + E2$
	1152.73(34)	1.7(2)	$9^+ \rightarrow 7^+$	1.03(15) ^f	0.09(4)	$E2$
	1272.1(5)	0.30(4)	$9^+ \rightarrow 8^+$	0.80(9) ^t		($M1 + E2$)
	5062.5(5)	274.50(31)	0.25(3)	(11^+) \rightarrow 10^+	0.75(6) ^t	
5114.9(5)	1065.60(36)^m	0.22(3)	$\rightarrow 8^-$			
5540.3(4)	444.40(32)	0.21(2)	$11^- \rightarrow (10^-)$			[$M1 + E2$]
	1127.10(36)	2.2(1)	$11^- \rightarrow 9^-$	1.10(6) ^e	0.10(7)	$E2$
5689.9(4)	830.5(5)	0.20(2)	$11^+ \rightarrow 9^+$			[$E2$]
	902.10(44)	0.45(5)	$11^+ \rightarrow 10^+$	0.51(4) ^q	-0.08(5)	$M1 + E2$
5785.2(4)	997.30(44)	0.16(2)	$12^+ \rightarrow 10^+$			[$E2$]
	1159.20(36)	1.8(2)	$12^+ \rightarrow 10^+$	1.07(4) ^r	0.11(6)	$E2$
6807.6(5)	1022.50(40)	0.22(4)	$\rightarrow 12^+$			
	1117.4(5)	0.10(5)	$\rightarrow 11^+$			
7078.1(6)	1292.90(45)	1.34(12)	$14^+ \rightarrow 12^+$	1.06(12) ^s	0.09(8)	$E2$
8466.1(8)	1388.0(5)	0.40(5)	$16^+ \rightarrow 14^+$	1.09(16) ^s	0.11(6)	$E2$

^aDeduced from the ground-state-feeding 614-keV transition, $E2$ gate.

^bDeduced from the 889($4^+ \rightarrow 2^+$)-keV, $E2$ gate.

^cDeduced from the 882-keV, $E2$ gate.

^dDeduced from the 1309-keV, $E2$ gate.

^eDeduced from the 950-keV, $E2$ gate.

^fDeduced from the 969-keV, $E2$ gate.

^gDeduced from the 633-keV, $E2$ gate.

^hDeduced from the 741-keV, $E2$ gate.

ⁱDeduced from the 271-keV, $E2$ gate.

^jDeduced from the 1044-keV, $E2$ gate.

^kDeduced from the 1575-keV, $E2$ gate.

^lDeduced from the 1285-keV, $E2$ gate.

^mTentatively placed in the level scheme.

ⁿDeduced from the 1894-keV, $E1$ gate.

^oDeduced from the 383-keV, $E2$ gate.

^pDeduced from the 1153-keV, $E2$ gate.

^qDeduced from the 956-keV, $E2$ gate.

^rDeduced from the 1039-keV, $E2$ gate.

^sDeduced from the 1040+1159-keV, $E2$ sum gate.

^tDue to the presence of close-lying energy, the quoted DCO ratio could not be extracted unambiguously.

As an electric transition preferentially scatters in the perpendicular direction, a positive Δ_{asym} value is obtained for such a transition. The negative Δ_{asym} value of a transition would indicate its magnetic nature. A nearzero value of Δ_{asym} of a transition is indicative of mixed multipole character for the transition. However, for a typical $\Delta J = 0$ transition, the negative (positive) value of Δ_{asym} represents $E1$ ($M1$)

nature of the transition. The four clover detectors of the array placed at 90° have been effectively used for extracting the Δ_{asym} values. The extracted Δ_{asym} values for the newly assigned multiplicities of the transitions belonging to ^{78}Se are depicted in Fig. 4. The transitions having electric, magnetic, and mixed characters can clearly be identified from the figure.

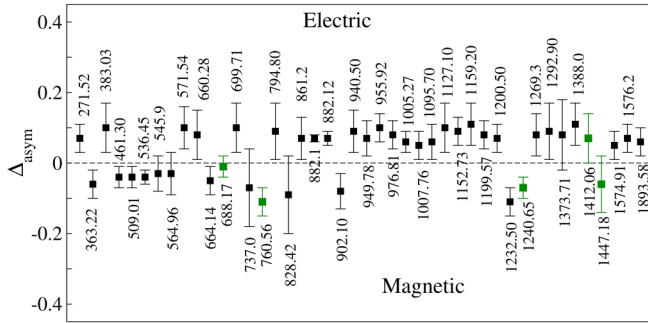


FIG. 4. The experimental asymmetry (Δ_{asym}) values for a few of the transitions of ^{78}Se obtained from the polarization measurement. The green data points belong to $\Delta J = 0$ transitions. The dotted line through the zero value of asymmetry has been drawn to guide the eye.

III. EXPERIMENTAL RESULTS

Based on $\gamma\gamma$ coincidence analysis, the level scheme of ^{78}Se has been established up to $E_x \approx 8.5$ MeV and $J = 16\hbar$, and is presented in Fig. 5. The observed level scheme from

the present investigation is found to be in good agreement with that from the previous work of Schwengner *et al.* [7]. However, an extension to the previously known level scheme has been made in the present work by placing 39 new transitions. The newly observed transitions are indicated with red color in Fig. 5. The excited levels have been categorized under five different groups as shown in Fig. 5. It is worth mentioning that an extensive effort was made to deal with the complexity of the level scheme of ^{78}Se arising mainly due to the presence of several close-lying doublet transitions. Different gating transitions were used for determining the relative intensity, DCO, and Δ_{asym} values of the close-lying doublet transitions. The newly found spectroscopic results are summarized in Table I. The quoted uncertainties for γ -ray energies comprise statistical and systematic uncertainties. The uncertainties associated with DCO and Δ_{asym} values are statistical only. The uncertainties for the intensities of the gamma transitions are expressed by adding in quadrature a 5% uncertainty for efficiency correction to the corresponding statistical uncertainties. A necessary discussion of the specific findings related to a few positive and negative parity levels is put forward in the following subsections.

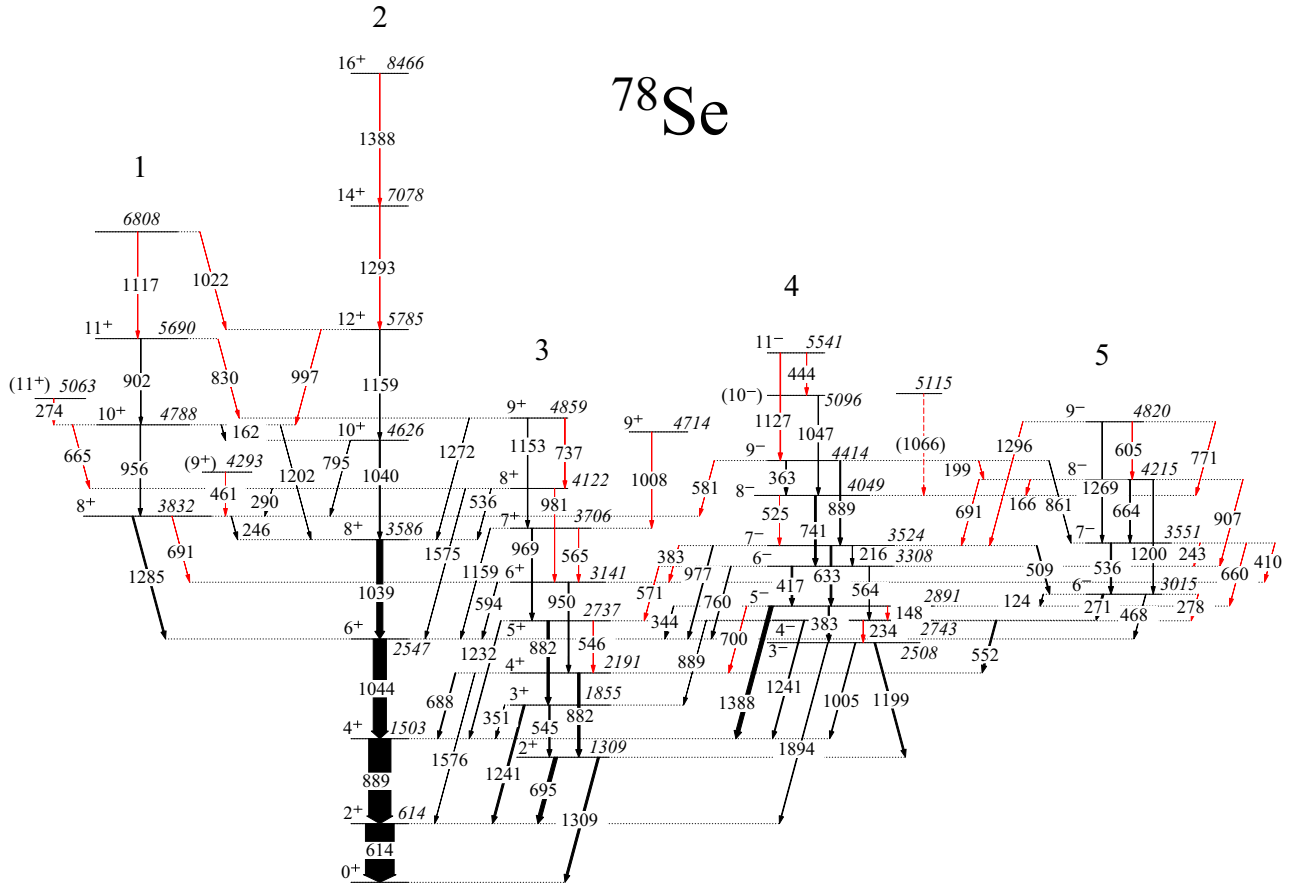


FIG. 5. The partial level scheme of ^{78}Se obtained from the present investigation. The newly observed transitions are indicated with red color. The level and transition energies are expressed in keV. The widths of the arrows are proportional to the intensities of the concerned transitions. The tentatively assigned transitions are indicated by dotted arrows. The tentative spin-parity assignments of the levels are expressed in parentheses.

A. Positive parity levels

Tentative spin-parity assignments of (10^+) and (12^+) were made respectively for the 4626- and 5785-keV levels in the previous investigation [7]. The extracted values of DCO and Δ_{asym} for the 795- and 1159-keV transitions, decaying from the 4626- and 5785-keV levels respectively, are suggestive of $E2$ multiplicities. Hence, firm 10^+ and 12^+ assignments for the 4626- and 5785-keV levels have been made in the present investigation. It is also to be noted here that the ground state positive parity band was known up to $E_x = 5785$ keV and $J^\pi = 12^+$ prior to the present investigation. The previously known ground state band has been extended up to $E_x = 8466$ keV and $J^\pi = 16^+$ due to the placements of two additional 1293- and 1388-keV $E2$ transitions that feed the 12^+ , 5785-keV and 14^+ , 7078-keV levels, respectively (see band 2 of Fig. 5). The extracted DCO and Δ_{asym} values along with the observed decay pattern confirms the $\Delta J = 2$, $E2$ multiplicities for the 1293- and 1388-keV transitions. The confirmed spin-parity assignments of the two newly observed levels as 14^+ and 16^+ have thus been made. It is to be pointed out here that the level scheme deduced from the present investigation comprises several close-lying levels with the same spin-parity assignments. These include three 8^+ levels at 3586, 3832, and 4122 keV; two 9^+ levels at 4714 and 4859 keV; and two 10^+ levels at 4626 and 4788 keV. The spin-parity assignments of all the concerned levels are confirmed from the analysis of the angular correlation and polarization data. An attempt has been made to find out all the probable decay transitions from the concerned levels within the sensitivity limit of present investigation. Two additional very weak 691- and 981-keV decay branches have been newly assigned to the 8_2^+ , 3832-keV and 8_3^+ , 4122-keV levels, respectively. The 9^+ , 4714-keV level has newly been placed in the decay scheme. Also, an additional 737-keV decay branch from the 9^+ , 4859-keV level has newly been established from the present investigation. In addition to the placements of additional weak decay branches, the $\gamma\gamma$ coincidence analysis of the present set of data is also found to be very helpful for the firm placements of a few transitions, which were tentatively placed in the previous investigation [7], decaying from the positive parity levels. These include 1159-, 1273-keV transitions of band 3 and 1202-, 795-keV transitions of sequence 1. Further, the assignments of J^π to the 2737-, 3141-, 3706-, and 4859-keV levels of band 3 were tentatively made as 5^+ , 6^+ , 7^+ , and 9^+ respectively, in the previous work of Schwengner *et al.* [7]. The tentative assignments are probably due to the presence of the doublet 882-keV transitions that prevented the unambiguous spin-parity assignments to the 2737-keV level, and subsequently to the other higher levels of band 3 as well since the previous investigation [7] measured the angular anisotropy and polarization asymmetry of the transitions from singles measurements. The DCO values, measured in the present work, are found to be 0.89(8) and 1.01(8) (see Table I) for the 882-keV transitions decaying from the 2191- and 2737-keV levels, respectively. As can be seen from Table I, two different parallel gating transitions of known $E2$ multiplicities have been used for accurate determination of the DCO values. Hence, unambiguous $E2$ multipolarity assignments have been made to both the

882-keV transitions. These assignments are further corroborated with the coincidence polarization asymmetry measurements. Thus a confirmed J^π assignment of 5^+ has been made for the 2737-keV level.

As mentioned in Sec. II, one LEPS detector was also used in the array for efficient detection of the low-energy transitions. A $\gamma\gamma$ matrix comprising the events from LEPS detectors in one axis and the recorded events from the clover detectors in other axis was also constructed. However, the coincidence LEPS spectrum generated from the gate on the ground-state-feeding 614-keV transition recorded by the clover detectors does not indicate the presence of any low-energy transitions as such with $E_\gamma < 124$ keV. Hence, no additional low-energy decay branches with $E_\gamma < 124$ keV are placed in the level scheme. As can be seen from Fig. 5, sequence 1 comprising positive parity levels has also been extended to 6808 keV level. Several decay paths of sequence 1 to the other two positive parity bands 1 and 3 are also newly established.

B. Negative parity levels

The negative parity levels have been grouped under bands 4 and 5. The grouping of the levels has been made based on the energy pattern of the levels, the spin sequences of the levels, and the decay pattern of the levels. Band 4 is built on the 3^- , 2508-keV level and has been extended up to the 11^- , 5540-keV level with the placements of two new decay branches from the level. The $E1$ multipolarity to the three newly observed 383-, 571-, and 700-keV transitions of band 4 have been made following the extracted DCO and polarization-asymmetry values of the transitions. The previously made tentative spin-parity assignments of the 4414-keV level of band 4 have also been confirmed from the present work. Hence, the confirmed spin-parity assignments for all the levels, except the (10^-) level at 5096 keV, of band 4 are made from the present investigation. Band 5 built on the 6^- , 3015-keV level comprises the 7^- , 3551-keV, 8^- , 4215-keV, and 9^- , 4820-keV levels. The spins and parities of the levels were tentatively assigned in the previous investigation by Schwengner *et al.* [7]. The confirmed spin-parity assignments for the levels of the band could be made in the present investigation due to the placements of several new decay branches and their followup DCO and polarization measurements.

IV. DISCUSSION

As mentioned in the previous section, the level scheme of ^{78}Se has been extended both along the vertical and horizontal dimensions due to the placement of several new transitions. The spins and parities for a majority of the levels are also firmly established. Depending upon the decay patterns, the observed levels are grouped under different sequences (see Fig. 5). The characteristic features of different bands and the effects of quasiparticle (qp) alignments on the observed band structures are discussed in the following subsections.

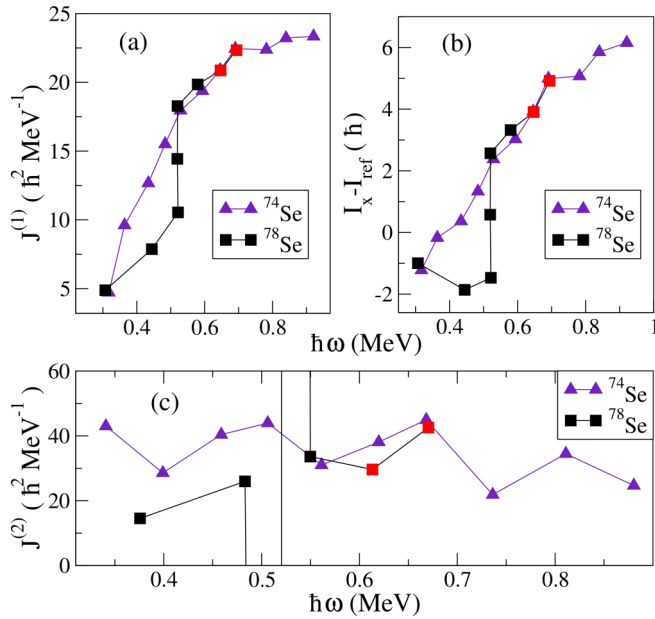


FIG. 6. Variation of (a) kinematic moment of inertia $J^{(1)}$, (b) the aligned angular momentum $I_x - I_{\text{ref}}$ ($= i_x$), and (c) dynamic moment of inertia $J^{(2)}$ as a function of rotational frequency $\hbar\omega$ for the yrast positive parity ground state bands in $^{74,78}\text{Se}$. The reference angular momentum has been parametrized as $I_{\text{ref}} = 21\omega - 3$ [17–19]. The newly extracted data points are indicated with red color.

A. Level structure of yrast positive parity ground state band (band 2)

Due to the occupancy in both the proton and neutron $1g_{9/2}$ intruder orbitals, it is expected that the yrast level structure of ^{78}Se should exhibit the consequent effects arising from the 2qp $\nu(1g_{9/2}^2)$ and $\pi(1g_{9/2}^2)$ alignments. The spectroscopic information of the newly extended ground state band structure of ^{78}Se has been used to show the rotational frequency ($\hbar\omega$) dependent variation of the kinematic moment of inertia, $J^{(1)}$, aligned angular momentum, $I_x - I_{\text{ref}} = i_x$ (Harris parameters used for the reference configuration has been taken from Ref. [17]), and dynamic moment of inertia, $J^{(2)}$, in Fig. 6. The relevant data corresponding to the neighboring ^{74}Se nucleus are also plotted in the figure for the sake of comparison. As can be seen from Fig. 6(a), there is a difference in the rising pattern for $J^{(1)}$ values for $^{74,78}\text{Se}$ up to $\hbar\omega \approx 0.55$ MeV. Above the rotational frequency of 0.55 MeV, the variation pattern of $J^{(1)}$ appears to be similar for the two nuclei $^{74,78}\text{Se}$. Such features corroborate well the alignment plots of Fig. 6(b).

Further, it can be seen from Fig. 6(c) that the first peak, due to the alignment of a pair of quasiparticles, occurs at $\hbar\omega \approx 0.55$ MeV for both $^{74,78}\text{Se}$. The second peaklike structure for ^{74}Se is clearly seen at $\hbar\omega \approx 0.65$ MeV, indicating the occurrence of another quasiparticle-pair alignment. However, the position of the second distinct kinklike structure for ^{78}Se cannot be localized in Fig. 6(c) due to the unavailability of additional high-spin data points. Considering the structural similarities between ^{74}Se and ^{78}Se , it can be suggested from the present investigation that the second alignment for the pair

of quasiparticles in ^{78}Se should occur at a rotational frequency $\hbar\omega \gtrsim 0.65$ MeV. These facts indicate the occurrence of two well-separated successive band crossing phenomena along the ground state positive parity bands of $^{74,78}\text{Se}$.

In order to investigate the nature of quasiparticle alignments and their subsequent possible shape change phenomena, the total Routhian surface (TRS) calculations for ^{78}Se were performed. The calculations were carried out following the prescriptions as described in Refs. [20,21]. The surfaces obtained in the β_2 - γ plane from TRS calculations at two different rotational frequencies are shown in Fig. 7. Figures 7(a) and 7(b) demonstrate the shape of the nucleus at $\hbar\omega = 0.30$ and 0.55 MeV, which correspond to the respective frequencies before and after the experimentally observed regime of the first band crossing [see Fig. 6(c)]. It can be seen from Fig. 7(a) that the TRS at $\hbar\omega = 0.30$ MeV indicates a triaxial shape with $\beta_2 \approx 0.30$ and $\gamma \approx -33^\circ$. The changing scenario after the first band crossing can clearly be observed in Fig. 7(b). The TRS at $\hbar\omega = 0.55$ MeV shows the presence of two minima in the energy surface. The first minimum is found to be associated with the shape parameters, $\beta_2 \approx 0.30$, $\gamma \approx +49^\circ$, while the shape parameters obtained for the second minimum are $\beta_2 \approx 0.30$, $\gamma \approx -27^\circ$. Thus, it can be surmised that the triaxial shape in ^{78}Se seems to persist before and after the observed first band crossing regime of the positive parity ground state band (band 2). However, the occurrence of $\nu(1g_{9/2}^2)$ qp alignment seems to drive the nucleus from a triaxial shape with negative γ value to a triaxial shape with positive γ value indicating thereby the nonrigid triaxial behavior. It is to be pointed out here that the calculated shape change phenomena for ^{74}Se (see [8]) and ^{78}Se are found to be quite different. While there is a distinct change of shape from prolate to triaxial observed for ^{74}Se with the increasing spins [8], the triaxial shape for ^{78}Se seems to develop in the spin regime even before the first band crossing. The occurrence of similar triaxial shapes (see the values of $\beta_2 = 0.30^\circ$ and $\gamma = 49^\circ, -27^\circ$ for ^{78}Se obtained from the present calculation, and $\beta_2 = 0.29^\circ$ and $\gamma = 40^\circ, -26^\circ$ for ^{74}Se from Ref.[8]) after the first band crossing frequency at $\hbar\omega \approx 0.50$ MeV for both $^{74,78}\text{Se}$ gives rise to the observed similar behavior for the pattern of variation in $J^{(1)}$, i_x , and $J^{(2)}$ at the higher rotational frequencies with $\hbar\omega \gtrsim 0.50$ MeV [see Figs. 6(a), 6(b), and 6(c)].

Further, an attempt has been made to understand the type of quasiparticle alignments associated with the kinklike structures of $J^{(2)}$ [see Fig. 6(c)] observed at $\hbar\omega \approx 0.52$ and 0.65 MeV for ^{78}Se . In this context, the theoretical crossing frequencies ($\hbar\omega_c$) were determined from the calculated single particle Routhians for different values of triaxiality parameter (γ) while considering the value of the deformation parameter to be $\beta_2 = 0.28$. The crossing frequencies have been calculated for both $1g_{9/2}$ quasiprotons and quasineutrons, and the subsequent variations are shown in Fig. 8. The horizontal dotted lines have been drawn through the observed band crossing frequencies at $\hbar\omega \approx 0.52$ MeV and $\hbar\omega \approx 0.65$ MeV to guide the eye. It is obvious from the figure that the lower crossing is due to the alignment of a pair of $\nu(1g_{9/2})$ quasineutrons, whereas the alignment of a pair of $\pi(1g_{9/2})$ quasiprotons is likely responsible for the observed band crossing at $\hbar\omega \gtrsim 0.65$ MeV.

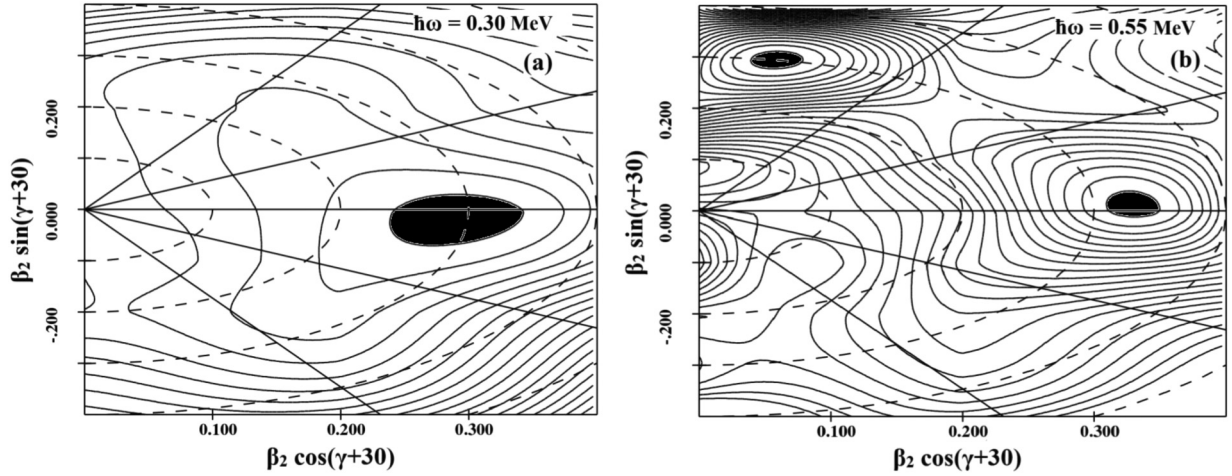


FIG. 7. Total Routhian surfaces (TRSs) plotted in the (β_2, γ) plane for the positive parity ground state band (band 2) of ^{78}Se . The plots are shown for two rotational frequencies at (a) $\hbar\omega = 0.30$ MeV and (b) $\hbar\omega = 0.55$ MeV, which correspond respectively to the situations before and after the crossing frequency due to $\nu(1g_{9/2}^2)$ alignments (see text for details). The energy separation between two consecutive contours is 400 keV.

The regime of the first and second band crossings in ^{78}Se due to neutron and proton pair alignments further gets confirmed from the systematics of the experimental band crossing frequencies extracted for the even-even Se isotopes, shown in Fig. 9. The presence of excess neutrons near the Fermi level seems to favor the first band crossing in ^{78}Se to be due to neutron alignment. Figure 9 also demonstrates the proton pair alignment as the favorable case for the first band crossing in ^{74}Se . However, the newly added data point in Fig. 9 (see the red marked filled circle) shows that the difference between the two successive crossing frequencies is found to be almost the same for $^{74,78}\text{Se}$.

B. Irregular sequence of positive parity levels (sequence 1)

Figure 5 indicates that the irregular positive parity sequence (sequence 1) develops in the level scheme of ^{78}Se at an excitation regime of $E_x \approx 3.8$ MeV with $J^\pi = 8^+$. The observed irregular sequence preferentially decays to the ground state positive parity band (band 2). Also, it is interesting to note that the irregular sequence appears at the periphery of the excitation regime of 2qp alignment from the $1g_{9/2}$ neutrons. Considering the measured lifetime values from Ref. [7] and incorporating the newly observed decay branches from the present investigation, the levels at 3832, 4788, 5690, and 6808 keV of sequence 1 are found to decay to the lower lying levels

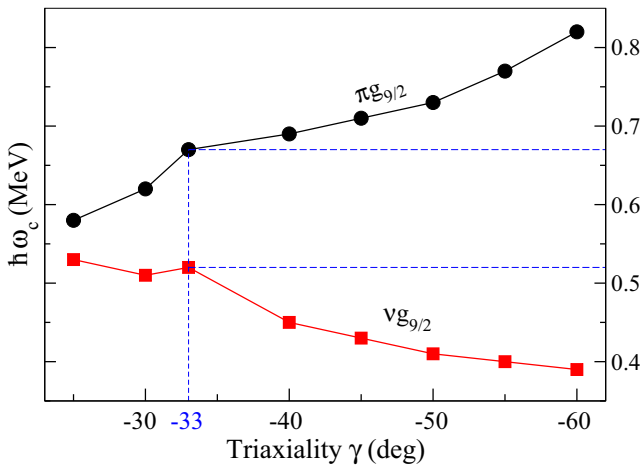


FIG. 8. Theoretical crossing frequencies ($\hbar\omega_c$) for ^{78}Se , obtained from TRS calculations, are plotted as a function of triaxiality parameter (γ). The blue dashed horizontal lines have been drawn through the region of experimentally observed crossing frequencies. See text for details.

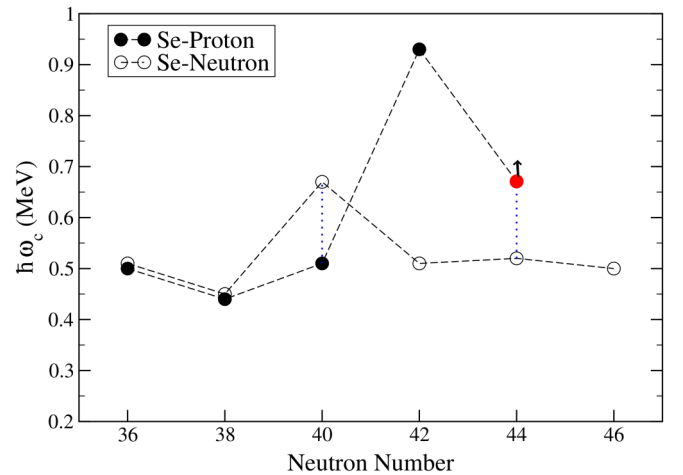


FIG. 9. The experimental crossing frequencies for the pairs of $1g_{9/2}$ proton and $1g_{9/2}$ neutron alignments plotted as a function of neutron number for a few even-even Se isotopes. The red marked data point corresponds to the new finding for ^{78}Se from the present investigation. The necessary data for the other nuclei are taken from Refs. [1,2,8,22–24]. The lines joining the data points have been drawn to guide the eye.

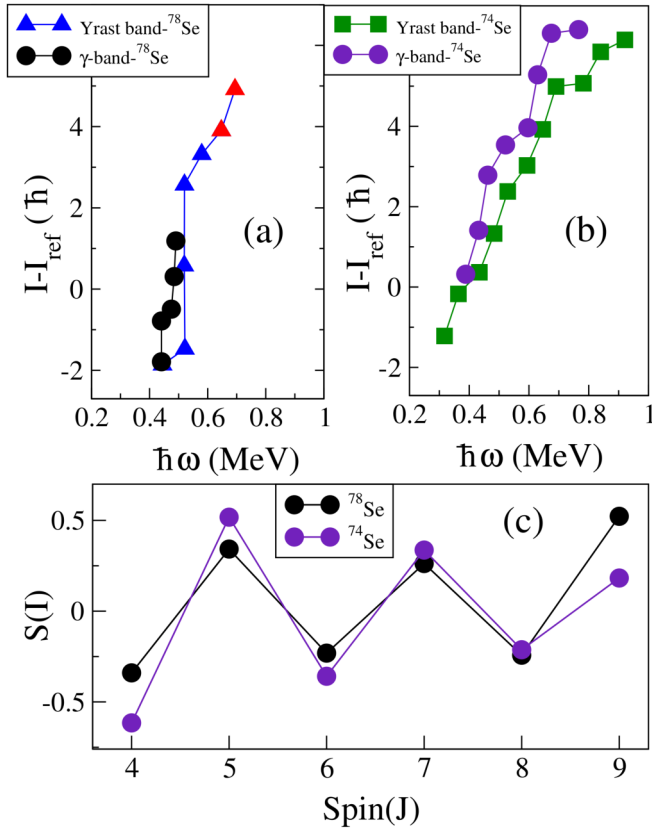


FIG. 10. Variation of (a) aligned angular momentum ($I - I_{\text{ref}}$) of band 2 (ground state band) and band 3 (gamma band) of ^{78}Se as a function of rotational frequency ($\hbar\omega$). The red circles are the data points newly added to band 2. The same has been plotted in panel (b) for ^{74}Se . Panel (c) demonstrates the experimental variation of the staggering parameter, $S(I)$, for ^{78}Se as a function of spin (J).

of band 2 with the values of $B(E2) \lesssim 10$ W.u.. This suggests the noncollective feature of sequence 1.

C. Positive parity band built on the 2_2^+ , 1309 keV state (band 3): Evolution of the γ band

The experimental data obtained from the present investigation do not permit us to extend band 3 beyond the previously known 9^+ , 4859 keV state. But even with the available limited spectroscopic information, a similar pattern of variation is found to persist for bands 2 and 3 [see Fig. 10(a)]. It is obvious from Fig. 10(a) that both bands exhibit the occurrence of two-quasineutron $1g_{9/2}$ alignment at $\hbar\omega \approx 0.5$ MeV. The observed similarity in the variation of the aligned angular momenta of band 3 with that of the ground state positive parity band (band 2) supports the γ vibrational feature for band 3 [25–27]. An identical feature exists between the ground state band and the excited γ band built on the 2_2^+ , 1269-keV state of ^{74}Se and has been depicted in Fig. 10 (b).

To further investigate the nature of band 3, the staggering parameter for the different levels of the band has been extracted using the following relation and plotted in

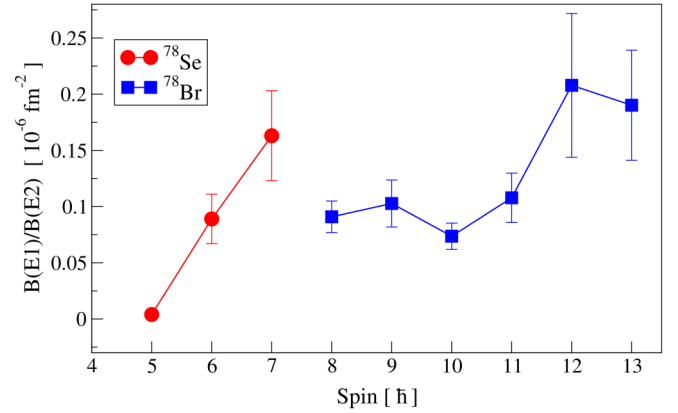


FIG. 11. The variation of experimental $B(E1)/B(E2)$ values plotted as a function of spin (I) for the octupole correlated band structures in ^{78}Se and ^{78}Br . The red circles are the new data points for ^{78}Se extracted from the present investigation.

Fig. 10(c):

$$S(I, I-2) = \frac{[E(I) - E(I-1)] - [E(I-1) - E(I-2)]}{E(2_2^+)}. \quad (1)$$

As can be seen from the figure, the staggering pattern for ^{78}Se looks similar to that of ^{74}Se . The observed variation of $S(I)$ is suggestive of gamma-soft nature of the observed level structure of ^{78}Se built on the 2_2^+ , 1309-keV state. The experimental value of $\frac{E(2_2^+)}{E(2_1^+)} = 2.1$ for ^{78}Se further suggests that the shape of the nucleus is near the maximum triaxiality with $\gamma \approx 30^\circ$ following the Davydov-Fillipov (DF) model [28]. Hence, the onset of this near-maximum triaxial shape seems to occur at the periphery of the bandhead energy of band 3. This corroborates the results from the TRS calculations as discussed in Sec. IV A and the previous investigation carried out with Coulomb excitation measurement [29].

D. Negative parity band built on the 3_1^- , 2508 keV state (band 4): Onset of octupole correlation

The negative parity levels of band 4, built on the 3_1^- , 2508 keV state, decay to the positive parity levels of band 3 via several $E1$ transitions. A few of these interband linking $E1$ transitions were known from the previous work of Schwengner *et al.* [7]. A few additional $E1$ decay branches have been newly placed from the present investigation. In order to search for the onset of the octupole correlation effect in ^{78}Se , the experimental values of $B(E1)/B(E2)$ have been extracted for the transitions decaying from different excited levels of band 4 and are depicted in Fig. 11. For the sake of comparison, the previously measured $B(E1)/B(E2)$ values for the neighboring isobaric ^{78}Br nucleus are also incorporated in the figure. We pointed out here that the presence of octupole correlations in ^{78}Br has already been ascertained from the previous work of Ref. [30] based on the measured $B(E1)/B(E2)$ values. Figure 11 indicates that the measured values of $B(E1)/B(E2)$ for ^{78}Se are very similar to those of

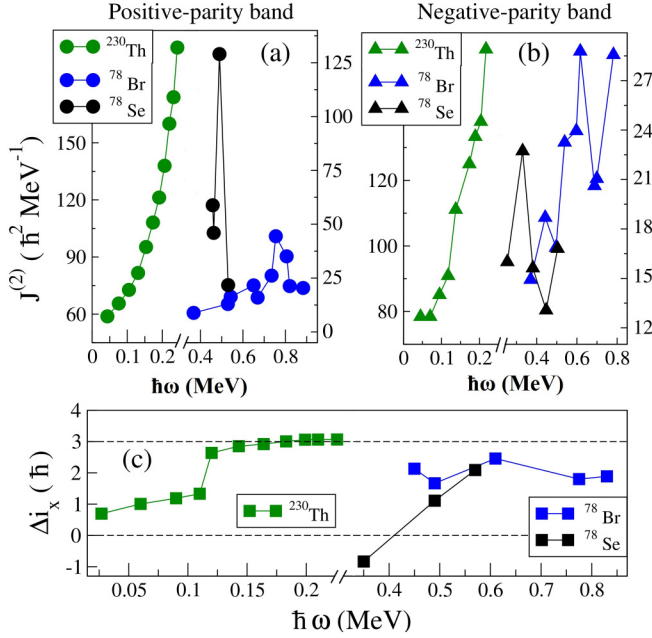


FIG. 12. Variation of dynamical moment of inertia $J^{(2)}$ plotted as the function of rotational frequency $\hbar\omega$ for (a) positive parity band (gamma band in cases of ^{78}Se , ^{78}Br and ground state band in the case of ^{230}Th [34]) and (b) negative parity octupole correlated band structure of ^{78}Se , ^{78}Br , and ^{230}Th . Panel (c) shows the variation in the difference in alignment Δi_x between the gamma band and octupole-correlated band plotted against $\hbar\omega$ for the nuclei ^{78}Se , ^{78}Br , and that between the ground state positive parity band and octupole band of ^{230}Th . The dashed horizontal lines have been drawn to guide the eye (see text for details).

^{78}Br . Hence, the octupole correlation effect seems to persist in ^{78}Se as well within the observed medium-spin excitation regime. An identical pattern of increasing trend in the $B(E1)/B(E2)$ values for the two the nuclei is obvious from the figure. However, the enhancement of $B(E1)/B(E2)$ values for ^{78}Se prevails in the lower spin regime.

Further, the consequences arising from the effect of quasiparticle alignments of the octupole correlated bands are distinctly visible in Fig. 12. It is obvious from Figs. 12(a) and 12(b) that the $J^{(2)}$ values for all the bands under consideration, except that for ^{230}Th , do not vary smoothly with the rotational frequencies, $\hbar\omega$. As discussed in Ref. [31], the values of Δi_x for smoothly varying bands are expected to approach either of the two feasible extreme values, zero and $3\hbar$, characterizing thereby the onset of stable octupole deformation and octupole vibrational feature, respectively. Here, Δi_x is the difference in aligned angular momentum and is defined as $\Delta i_x = i_x^- - i_x^+$, where i_x^- and i_x^+ are the experimental alignments of the concerned negative and positive parity bands, respectively. Thus, Fig. 12(c) points to the fact that ^{230}Th is a good example of octupole vibrators. The presence of alignments of a pair of quasiparticles in the concerned positive parity bands is found to be quite obvious at $\hbar\omega \approx 0.5$ MeV and $\hbar\omega \approx 0.8$ MeV for ^{78}Se and ^{78}Br , respectively [see Fig. 12(a)]. No such signatures for specified alignments are observed in the negative parity bands for ^{78}Se and ^{78}Br [see Fig. 12(b)].

Figure 12(c) demonstrates that both the ^{78}Se and ^{78}Br isobars attain a maximum value of $\Delta i_x \approx 2\hbar$. Hence, as suggested in Refs. [32,33], the presence of a quasiparticle-pair alignment in one of the partners of the octupole correlated bands possibly provides hindrance to attaining a maximum $3\hbar$ value of Δi_x , and hence the observed level structures of ^{78}Se and ^{78}Br cannot be considered to be the ideal examples of perfect octupole vibrators.

E. Negative parity band built on the 6_2^- , 3015-keV level (band 5)

The experimental data suggest that this negative parity band was populated very weakly in the present investigation. Hence, it was not possible to extend the bandlike structure beyond the 9^- , 4820-keV level. This bandlike structure is found to possess several interesting features: (a) the energy of the bandhead is quite high and lies at the excitation regime close to the periphery of first band crossing, (b) a higher value of $B(M1)/B(E2)$ is observed for decay of the intraband transitions in comparison to what have been found for the intraband transitions belonging to the other bands, (c) the band decays to both the positive- and negative parity yrast bands, and (d) the signature splitting appears to be very small. Such excited negative parity bands with bandheads at $E_x > 2$ MeV and $J^\pi \geq 13/2^-$ were previously reported in several neighboring odd-mass nuclei belonging to the $A \approx 80$ region [35,36] and categorized as high- K bands. The configuration for this type of excited negative parity band for $^{77,79}\text{Br}$ -isotopes was suggested as $\pi(g_{9/2}) \otimes \nu(fp) \otimes \nu(g_{9/2})$ based on deformed shell model calculations [35]. Also, the negative parity $13/2^-$ band of the $^{77}\text{As}_{44}$ isotope was assigned in a previous work [36] as a 3qp band with a similar type of configuration. In addition to that, the high-lying negative parity dipole bands were also previously observed in $^{77,79}\text{Se}$ isotopes and interpreted as high- K bands with a 3qp configuration of $\pi[(1g_{9/2})(fp)] \otimes \nu[(1g_{9/2})]$ [37,38]. Considering the analogy in the observed decay pattern and the excitation energy and spin of the bandhead, band 5 of ^{78}Se can be assigned with a probable 4qp high- K bandlike structure having either $\pi[(1g_{9/2}^2)] \otimes \nu[(1g_{9/2})(fp)]$ or $\pi[(g_{9/2})(fp)] \otimes \nu[(g_{9/2}^2)]$ as the dominant configuration.

V. CONCLUSIONS

The results from a detailed spectroscopic investigation of the level structure of ^{78}Se in the medium-spin regime are reported in the present paper. The level scheme has been enriched with the placements of several new transitions decaying from yrast and non-yrast levels of both parities. Total Routhian surface (TRS) calculations have been carried out to interpret the experimentally observed results. The systematics in the crossing frequencies of Se isotopes have been unveiled and the difference in the crossing frequencies due to $\pi(1g_{9/2}^2)$ and $\nu(1g_{9/2}^2)$ quasiparticle alignments are found to be similar in the $^{74,78}\text{Se}$ nuclei. The ground state bands of $^{74,78}\text{Se}$ exhibit surprisingly similar types of features after the first crossing frequency, and this corroborates the persistence of similar types of triaxial shapes in the two nuclei in the higher spin regime. The effects of $1g_{9/2}$

neutron pair alignments on different possible modes of excitation such as γ vibration and octupole correlations have been presented. A four-quasiparticle high- K bandlike structure built on 6^- , 3015-keV level is newly proposed. The band is supposed to have a predominant contribution from either $\pi[(1g_{9/2}^2)] \otimes \nu[(1g_{9/2})(fp)]$ or $\pi[(g_{9/2})(fp)] \otimes \nu[(g_{9/2}^2)]$ configuration.

ACKNOWLEDGMENTS

The authors would like to gratefully acknowledge the help and cooperation received from all the participants for their joint effort in setting up the INGA facility at VECC, Kolkata.

Thanks are also due to the cyclotron operating staff of VECC, Kolkata for their excellent support during the experiment. The authors would also like to acknowledge the assistance of the target laboratory staff at VECC, Kolkata in preparing the targets. Financial support from the Department of Science and Technology (D.S.T.), Government of India (Grant No. IR/S2/PF-03/2003-II) is gratefully acknowledged. The authors, K.M. and A.C. sincerely acknowledge the financial assistance from IUAC, New Delhi through Project Code No. UFR-56317. One of the authors (A.C.) would also like to acknowledge the financial support and cooperation received from UGC-DAE CSR, Kolkata through Project No. UGC-DAE-CSR-KC/CRS/19/NP10/0921/0963. One of the authors (A.K.) acknowledges a grant received from the Institutions of Eminence (IoE), BHU (Grant No. 6031).

-
- [1] T. Mylaeus *et al.*, *J. Phys. G: Nucl. Part. Phys.* **15**, L135 (1989).
 [2] C. Xu *et al.*, *Phys. Rev. C* **91**, 061303(R) (2015).
 [3] J. Heese, D. J. Blumenthal, A. A. Chishti, P. Chowdhury, B. Crowell, P. J. Ennis, C. J. Lister, and C. Winter, *Phys. Rev. C* **43**, R921 (1991).
 [4] H. Sun, J. Döring, G. D. Johns, R. A. Kaye, G. Z. Solomon, S. L. Tabor, M. Devlin, D. R. LaFosse, F. Lerma, D. G. Sarantites, C. Baktash, D. Rudolph, C.-H. Yu, I. Y. Lee, A. O. Macciavelli, I. Birriel, J. X. Saladin, D. F. Winchell, V. Q. Wood, and I. Ragnarsson, *Phys. Rev. C* **59**, 655 (1999).
 [5] G. Mukherjee, H. C. Jain, R. Palit, P. K. Joshi, S. D. Paul, and S. Nagraj, *Phys. Rev. C* **64**, 034316 (2001).
 [6] T. Matsuzaki and H. Taketani, *Nucl. Phys. A* **390**, 413 (1982).
 [7] R. Schwengner *et al.*, *Z. Phys. A* **326**, 287 (1987).
 [8] J. Döring, G. D. Johns, M. A. Riley, S. L. Tabor, Y. Sun, and J. A. Sheikh, *Phys. Rev. C* **57**, 2912 (1998).
 [9] S. Das *et al.*, *Nucl. Instrum. Methods Phys. Res., Sect. A* **893**, 138 (2018).
 [10] D. C. Radford, *Nucl. Instrum. Methods Phys. Res., Sect. A* **361**, 297 (1995).
 [11] J. Theuerkauf, S. Esser, S. Krink, M. Luig, N. Nicolay, O. Stuch, and H. Wolters, Computer code Tv, Institute of Nuclear Physics, University of Cologne, 1993, <http://www.ikp.uni-koeln.de/fitz/>.
 [12] A. Krämer-Flecken *et al.*, *Nucl. Instrum. Methods Phys. Res., Sect. A* **275**, 333 (1989).
 [13] M. A. Jones *et al.*, *Rev. Sci. Instrum.* **69**, 4120 (1998).
 [14] R. Chakrabarti, S. Mukhopadhyay, Krishichayan, A. Chakraborty, A. Ghosh, S. Ray, S. S. Ghugre, A. K. Sinha, L. Chaturvedi, A. Y. Deo, I. Mazumdar, P. K. Joshi, R. Palit, Z. Naik, S. Kumar, N. Madhavan, R. P. Singh, S. Muralithar, B. K. Yogi, and U. Garg, *Phys. Rev. C* **80**, 034326 (2009).
 [15] E. S. Macias *et al.*, *Comput. Phys. Commun.* **11**, 75 (1976).
 [16] S. Nandi, G. Mukherjee, T. Roy, R. Banik, A. Dhal, S. Bhattacharya, S. Bhattacharyya, C. Bhattacharya, M. A. Asgar, H. Pai, S. Rajbanshi, P. Roy, T. K. Ghosh, K. Banerjee, T. K. Rana, S. Kundu, S. Manna, R. Pandey, A. Sen, S. Pal *et al.*, *Phys. Rev. C* **99**, 054312 (2019).
 [17] C. J. Gross *et al.*, *Nucl. Phys. A* **501**, 367 (1989).
 [18] P. K. Joshi *et al.*, *Nucl. Phys. A* **700**, 59 (2002).
 [19] J. Döring, G. D. Johns, R. A. Kaye, M. A. Riley, S. L. Tabor, P. C. Womble, and J. X. Saladin, *Phys. Rev. C* **52**, R2284 (1995).
 [20] W. Nazarewicz *et al.*, *Nucl. Phys. A* **435**, 397 (1985).
 [21] W. Nazarewicz *et al.*, *Nucl. Phys. A* **512**, 61 (1990).
 [22] N. Yoshinaga, K. Higashiyama, and P. H. Regan, *Phys. Rev. C* **78**, 044320 (2008).
 [23] G. Rainovski *et al.*, *J. Phys. G: Nucl. Part. Phys.* **28**, 2617 (2002).
 [24] S. M. Fischer, C. J. Lister, and D. P. Balamuth, *Phys. Rev. C* **67**, 064318 (2003).
 [25] A. Bohr and B. R. Mottelson, *Nuclear Structure*, Vol. II (World Scientific, Singapore, 1998).
 [26] J. Wang *et al.*, *Phys. Lett. B* **675**, 420 (2009).
 [27] S. Chakraborty *et al.*, *Eur. Phys. J. A* **55**, 46 (2019).
 [28] A. S. Davydov and G. F. Fillippov, *Nucl. Phys.* **8**, 237 (1958).
 [29] T. Hayakawa, Y. Toh, M. Oshima, A. Osa, M. Koizumi, Y. Hatsukawa, Y. Utsuno, J. Katakura, M. Matsuda, T. Morikawa, M. Sugawara, H. Kusakari, and T. Czosnyka, *Phys. Rev. C* **67**, 064310 (2003).
 [30] C. Liu, S. Y. Wang, R. A. Bark, S. Q. Zhang, J. Meng, B. Qi, P. Jones, S. M. Wyngaardt, J. Zhao, C. Xu, S. G. Zhou, S. Wang, D. P. Sun, L. Liu, Z. Q. Li, N. B. Zhang, H. Jia, X. Q. Li, H. Hua, Q. B. Chen *et al.*, *Phys. Rev. Lett.* **116**, 112501 (2016).
 [31] P. A. Butler *et al.*, *Nat. Commun.* **10**, 2473 (2019).
 [32] P. A. Butler, *Proc. R. Soc. A* **476**, 20200202 (2020).
 [33] P. A. Butler, L. P. Gaffney, P. Spagnoletti, K. Abrahams, M. Bowry, J. Cederkall, G. de Angelis, H. De Witte, P. E. Garrett, A. Goldkuhle, C. Henrich, A. Illana, K. Johnston, D. T. Joss, J. M. Keatings, N. A. Kelly, M. Komorowska, J. Konki, T. Kroll, M. Lozano, B. S. Nara Singh *et al.*, *Phys. Rev. Lett.* **124**, 042503 (2020).
 [34] J. F. C. Cocks *et al.*, *Nucl. Phys. A* **645**, 61 (1999).
 [35] S. L. Tabor *et al.*, *Phys. Scr.* **T56**, 175 (1995).
 [36] J. Doring, G. D. Johns, R. A. Kaye, K. W. Kemper, H. Sun, G. N. Sylvan, and S. L. Tabor, *Phys. Rev. C* **53**, 2674 (1996).
 [37] C. G. Li, Q. B. Chen, S. Q. Zhang, C. Xu, H. Hua, S. Y. Wang, R. A. Bark, S. M. Wyngaardt, Z. Shi, A. C. Dai, C. G. Wang, X. Q. Li, Z. H. Li, J. Meng, F. R. Xu, Y. L. Ye, D. X. Jiang, R. Han, C. Y. Niu, Z. Q. Chen *et al.*, *Phys. Rev. C* **100**, 044318 (2019).
 [38] G. D. Johns, J. Doring, R. A. Kaye, G. N. Sylvan, and S. L. Tabor, *Phys. Rev. C* **55**, 660 (1997).
 [39] https://www-nds.iaea.org/public/ensdf_pgm/.